SAND REPORT

SAND2004-4402
Unlimited Release
Printed September 2004

Chem-Prep PZT 95/5 for Neutron Generator Applications: Effects of Lead Stoichiometry on the Microstructure and Mechanical Properties of PZT 95/5

Chad S. Watson and Pin Yang

Prepared by
Sandia National Laboratories
Albuquerque, New Mexico 87185 and Livermore, California 94550

Sandia is a multiprogram laboratory operated by Sandia Corporation, a Lockheed Martin Company, for the United States Department of Energy under Contract DE-AC04-94AL85000.

Issued by Sandia National Laboratories, operated for the United States Department of Energy by Sandia Corporation.

Available to DOE and DOE contractors from
U.S. Department of Energy
Office of Scientific and Technical Information
P.O. Box 62
Oak Ridge, TN 37831

Telephone: (865)576-8401
Facsimile: (865)576-5728
E-Mail: reports@adonis.osti.gov
Online ordering: http://www.doe.gov/bridge

Available to the public from
U.S. Department of Commerce
National Technical Information Service
5285 Port Royal Rd
Springfield, VA 22161

Telephone: (800)553-6847
Facsimile: (703)605-6900
E-Mail: orders@ntis.fedworld.gov
Online order: http://www.ntis.gov/ordering.htm

SAND2004-4402
Unlimited Release
Printed September 2004

Chem-Prep PZT 95/5 for Neutron Generator Applications: Effects of Lead Stoichiometry on the Microstructure and Mechanical Properties of PZT 95/5

Chad S. Watson
Ceramic Materials Department

Pin Yang
Ceramics and Glass Processing Department

Sandia National Laboratories
P.O. Box 5800
Albuquerque, NM 87185-0889

ABSTRACT

The microstructure and mechanical properties of niobium-modified lead zirconate titanate (PNZT) 95/5 ceramics, where 95/5 refers to the ratio of lead zirconate to lead titanate, were evaluated as a function of lead (Pb) stoichiometry. Chemically-prepared PNZT 95/5 is produced at Sandia National Laboratories by the Ceramics and Glass Processing Department (14154) for use as voltage elements in ferroelectric neutron generator power supplies. PNZT 95/5 was prepared according to the nominal formulation of $Pb_{0.991+x}(Zr_{0.955}Ti_{0.045})_{0.982}Nb_{0.018}O_{3+x}$, where x ($-0.0274 \leq x \leq 0.0297$) refers to the mole fraction of Pb and O that deviated from the stoichiometric value. The Pb concentrations were determined from calcined powders; no adjustments were made to Pb compositions due to weight loss during sintering. The microstructure (second phases, fracture mode and grain size) varied appreciably with Pb stoichiometry, whereas the mechanical properties (hardness, fracture toughness, strength and Weibull parameters) exhibited modest variation. Specimens deficient in Pb, 2.74% (x = -0.0274) and 2.15% (x = -0.02150), had a high area fraction of a zirconia (ZrO_2) second phase on the order of 0.02. As the Pb content in solid solution increased the ZrO_2 content decreased; no ZrO_2 was observed for the specimen containing 2.97% excess Pb (x = 0.0297). Over the range of Pb stoichiometry most specimens fractured predominately transgranularly; however, 2.97% Pb excess PNZT 95/5 fractured predominately intergranularly. No systematic

changes in hardness or Weibull modulus were observed as a function of Pb content. Fracture toughness decreased slightly from 1.8 $MPa \cdot m^{1/2}$ for Pb deficient specimens to 1.6 $MPa \cdot m^{1/2}$ for specimens with excess Pb.

Although there are microstructural differences with changes in Pb content, the mechanical properties did not vary substantially. However, the average failure stress and fracture toughness for PNZT 95/5 containing 2.97% excess Pb decreased slightly. It is expected that additional increases in Pb content would result in further mechanical property degradation. The decrease in mechanical properties for the 2.97% Pb excess ceramics could be the result of a weaker PbO-rich grain boundary phase present in the material. If better mechanical properties are desired, it is recommended that PNZT 95/5 ceramics are processed by a method whereby any excess Pb is depleted from the final sintered ceramic so that near-stoichiometric values of Pb concentration are reached. Otherwise, a PbO-rich grain boundary phase may exist in the ceramic which could potentially be detrimental to the mechanical properties of PNZT 95/5 ceramics.

ACKNOWLEDGEMENTS

The authors gratefully acknowledge the members of the PZT Supply Team who provided considerable technical support during this study. Contributions by student interns Jason Kooi and Roman Wolf-Cecil are greatly appreciated. X-Ray diffractometry was performed by Mark Rodriquez, SEM and BSE analyses were performed by Dick Grant and Gary Zender, and Alice Kilgo and Don Susan provided image analysis support. Sandia is a multiprogram laboratory operated by Sandia Corporation, a Lockheed Martin Company, for the United States Department of Energy's National Nuclear Security Administration under Contract DE-ACO4-94-AL85000.

Intentionally Left Blank

CONTENTS

INTRODUCTION…….. 9
EXPERIMENTAL PROCEDURE……10
Powder Synthesis and Processing……10
Characterization……...10
RESULTS AND DISCUSSION……11
Calcined Powder……11
Zirconia Area Fraction…….....12
Fracture Mode……..14
Grain Size…….... 16
Hardness…….. 17
Fracture Toughness……..18
Strength and Weibull Parameters…….... 18
CONCLUSIONS…….…….... 21
REFERENCES…….. 21
APPENDIX……... 23

FIGURES

Fig. 1 The weight percent of monoclinic ZrO_2 in calcined powder decreases as Pb content increases (x = mol% Pb from the stoichiometric composition)……12
Fig. 2 Example of an (a) original backscattered electron image and (b) the binary image used for image analyses to obtain area fraction of ZrO_2 in polished PNZT 95/5 ceramics……... 13
Fig. 3 Area fraction of the monoclinic ZrO_2 second phase decreases with increasing Pb content. The ZrO_2 area fraction data are based on image analyses of cross-sectioned and polished specimens of PNZT 95/5 ceramics..... 14
Fig. 4 SEM micrographs showing fracture surfaces of the specimens (a) -2.74, (b) -2.15, (c) 0.51, (d) 1.38 and (e) 2.97% Pb from stoichiometry. The fracture mode is predominately transgranular for all of the specimens except for the 2.97% Pb excess specimen that failed predominately intergranularly…..…… 15
Fig. 5 Optical micrographs of etched PNZT 95/5 ceramics with corresponding binary images for grain size image analyses. A difference in grain size is seen when comparing the (a) low Pb (-2.74%) and the (b) high Pb (2.97%) specimens……..……..16
Fig. 6 The average grain size of PNZT 95/5 ceramics increases with increasing Pb content……..……..... 17
Fig. 7 Vickers hardness with 95% confidence limits does not deviate with increasing Pb content except for the specimen nearest stoichiometry (0.51% excess Pb)……...17
Fig. 8 Plot of fracture toughness as a function of Pb concentration.…….……..... 18
Fig. 9 Weibull plots of failure strength data for PNZT 95/5 ceramics with different Pb contents…….....20
Fig. 10 Average failure stress with 95% confidence intervals for PNZT 95/5……... 20

Fig. A Grain size distributions of PNZT 95/5 ceramics with different Pb concentrations. Grain size distributions are similar except the Pb excess specimens exhibit a slight tail for larger sized grains. The number fraction relates the number of grains within a specific size interval and is normalized by the total number of grains counted for the entire analysis…….....23

TABLES

TABLE I: Identification of PNZT 95/5 Specimens and Concentration of Pb in Calcined Powders…….…….10
TABLE II: Weibull Strength Parameters and Average Failure Stress with 95% Confidence Intervals…….20

INTRODUCTION

The production of PZT-based ceramics with reproducible composition can be complicated because of lead loss associated with the volatility of lead oxide at the temperatures used to sinter lead zirconate titanate (PZT) compacts.[1] To help compensate for Pb loss during calcination and sintering, excess Pb can be added to the batch formulation. In addition, Pb-containing burial powders can be used to help control Pb loss during sintering by equilibrating the PbO activity between the PZT compact and the atmosphere.[2-5] However, even with the use of excess Pb and burial powders, subtle variations in processing can result in PZT ceramics with varying Pb stoichiometry.

Deviations in Pb stoichiometry can have significant effects on the densification and microstructure of PZT-based ceramics.[5-9] Depending on the Pb concentration, liquid-phase or solid-state sintering mechanisms can dominate sintering kinetics. With excess Pb a PbO-rich liquid can form during the early stages of sintering resulting in particle rearrangement and solution-precipitation mechanisms leading to rapid densification.[9-11] If the PbO-rich liquid is not completely depleted during the final stages of sintering, a PbO-rich second phase can become trapped at grain boundaries and/or triple points during cool down.[10-12] Deficiencies in Pb content can cause zirconia (ZrO_2) phases to develop during sintering.[13]

Variations in composition, density and microstructure can significantly influence the electrical properties of PZT-based ceramics. For instance, second phases and porosity degrade the electro-optic properties of transparent lanthanum-modified lead zirconate titanate (PLZT) because of reduced optical transmittance,[6] whereas, the electromechanical properties of PZT can be enhanced with increased density and grain size, but degrade with the formation of second phases.[8, 13]

Although considerable work has been performed on the effects of Pb stoichiometry on the electrical properties of PZT, the influence of Pb content on the mechanical properties of PZT has received less attention.[14, 15] Furthermore, because of the enhanced electromechanical properties of PZT with compositions near the morphotropic phase boundary and the unique electro-optic properties of optically transparent PLZT most studies of the effect of Pb stoichiometry on electrical[6-8, 15] and mechanical properties[15] have been based near these technologically significant compositions. Our efforts, however, are concentrated on the effects of Pb deficiency and excess on the microstructure and mechanical properties of niobium-modified lead zirconate titanate (PNZT) 95/5. This composition is near the orthorhombic antiferroelectric (AFE) and rhombohedral ferroelectric (FE) phase boundary. Recent work by Yang *et al*[16] found that slight changes in Pb stoichiometry resulted in significant changes in the coercive field, the pressure required to induce the FE-to-AFE phase transformation and the charge storage capacity.

EXPERIMENTAL PROCEDURE

Powder Synthesis and Processing

Five niobium-modified lead zirconate titanate (PNZT) 95/5 batches, with a nominal composition of $Pb_{0.991+x}(Zr_{0.955}Ti_{0.045})_{0.9820}Nb_{0.018}O_{3+x}$, where x refers to the amount of Pb and O deviating from stoichiometry, were prepared with 0.5 to 4.5 mol% excess Pb to compensate for Pb loss during processing. PNZT 95/5 powders were prepared using a coprecipitation method,[17, 18] where lead acetate/glacial acetic acid solutions were mixed with Zr, Ti, Nb n-butoxides/glacial acetic acid solutions to form a metal cation solution. The coprecipitation reaction was carried out by adding an oxalic acid/n-propanol solution to the metal cation solution. The precipitant suspension was vacuum filtered and then the precipitant slurry was dried. The precursor powder was pyrolyzed at 400°C for 16 hr, dry ball-milled with 19 mm ZrO_2 media for 1 hr and then calcined at 900°C for 16 hr. After calcination, 0.9 wt% of sub-125 μm spherical polymerized methyl methacrylate (lucite) was mixed into the powder. The powder was then granulated by adding 2 wt% binder (HA4) in a dilute aqueous solution while being tumbled in a v-blender; followed by drying at 80°C for 16 hr. Rectangular powder compacts were formed by uniaxially pressing ~150 gm of powder at 96 MPa. To remove the organic additives, the powder compacts were slowly heated to 750°C and held at temperature for 4 hr. To help prevent Pb loss, a double-crucible technique with PNZT 95/5 burial powder was used in an attempt to equilibrate the PbO vapor pressure in the surrounding atmosphere during sintering. Specimens were sintered at 1350°C for 6 hr.[19] Weight loss, presumably due to PbO volatilization during sintering, was typically less than 0.2%.

Characterization

X-ray diffractometry (Siemens, D500) was used to identify phases in the calcined powder. The 2θ angle ranged from 20° to 100° with a step size of 0.04° and a counting time of 20 s/step. Both low-temperature rhombohedral PNZT and monoclinic ZrO_2 were identified in the calcined powders. Chemical analyses of the calcined powders were performed using the inductively coupled plasma-atomic emission spectrometry (ICP-AES) technique. The ICP-AES data were used to determine the Pb concentration in the calcined powder that was either deficient or in excess of stoichiometry (Table I).

Polished, unetched specimens were examined using a scanning electron microscope (Hitachi S-4500) with a backscattered electron (BSE) detector to locate second phases in sintered PNZT 95/5 ceramics. Image analyses of the BSE images were performed to

TABLE I: Identification of PNZT 95/5 Specimens and Concentration of Pb in Calcined Powders

Batch	Hi Fire #	Pb Content (mol)	Mol% Pb Excess/Deficient (x) from Stoichiometry
TSP 68	997	0.9961	0.51
TSP 69	999	1.0204	2.97
TSP 70-2	1003	1.0047	1.38
TSP 75-A	1011	0.9697	-2.15
TSP 75-B	1013	0.9638	-2.74

quantify the area fraction of second phases as a function of Pb content. Fracture surfaces were examined with a scanning electron microscope (SEM) for fracture mode determination. Sintered PNZT 95/5 ceramics from each Pb batch were polished and chemically etched for grain size measurements. Grain size was determined using image analysis (Imagist Software, Version 10, Princeton Gamma-Tech Inc., Rocky Hill, New Jersey) by measuring the average directed diameters of each grain. This technique takes twelve measurements at 30° increments for each grain and is most suitable for specimens that consist of equiaxed grains. A total of 1200-1700 grains was sampled for each specimen.

Hardness, fracture toughness, strength and Weibull parameters were evaluated for each Pb content. For hardness and toughness measurements, a Vickers diamond indentor contacted an optically polished specimen for 15 sec with a peak load of 19.6 N. Toughness measurements were made by measuring the average length of the radial cracks (*2c*) emanating from the hardness impression. The indentation crack-length fracture toughness[20] was obtained with the following equation:

$$K_{Ic} = 0.016\left(\frac{E}{H}\right)^{\frac{1}{2}} \bullet \left(\frac{P}{c^{\frac{3}{2}}}\right) \qquad (1)$$

where E is the modulus and P (N) is the indentation load. The modulus was assumed to be 110 GPa.[21] The hardness value incorporated in Eq. 1, defined as the peak indentation load divided by the projected contact area, is given by $H = 2P/d^2$ where d (mm) is the average length of the two diagonals. Bend bars were sliced and ground from the sintered compacts and finished to dimensions with a 600 grit diamond wheel. Strength was measured according to ASTM C1161-02a, except the distances between the inner loading points and outer supports were 9 and 18 mm. Weibull parameters were calculated from the room temperature strength data. All PNZT 95/5 specimens were tested in the unpoled condition.

RESULTS AND DISCUSSION

Calcined Powder

X-ray diffraction (XRD) results indicated that prior to calcination the oxalate powder is amorphous and after calcination the powder has crystallized into a perovskite phase (low-temperature rhombohedral PNZT) with a minor secondary phase (monoclinic ZrO_2). As shown in Fig. 1, the ZrO_2 wt%, determined by quantitative XRD using the Rietveld refinement method, decreases with increasing Pb content. The ZrO_2 second phase was detected in all compositions, including those with excess Pb as measured by ICP-AES. Prior to calcination, the ZrO_2 second phase is not found in the powders suggesting that ZrO_2 developed during calcination. The monoclinic ZrO_2 second phase may be attributed to compositional fluctuations in localized regions in the powder as a result of poor homogenization during synthesis and a subsequent milling operation. Also, because of

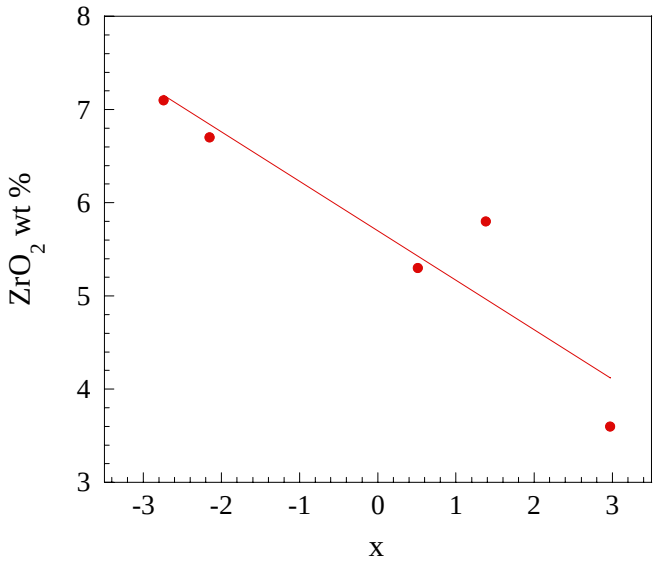

Fig. 1 The weight percent of monoclinic ZrO_2 in calcined powder decreases as Pb content increases (x = mol% Pb from the stoichiometric composition).

the long (16 hr) and relatively high temperature (900°C) calcination step, localized regions of Pb loss may have resulted in the formation of ZrO_2 precipitates in the calcined powder. Furthermore, uncertainties in the ICP-AES technique may have resulted in the overestimation of Pb. If Pb was overestimated, then the presence of ZrO_2 in the calcined PZT powders would be expected.

Zirconia Area Fraction

Because of the volatility of PbO at the high temperatures (1350°C) used for sintering, a Pb-containing burial powder must be used to mitigate the loss of Pb in the PZT compact. During sintering with a burial powder, PNZT 95/5 compacts typically lose 0.2% weight. This may be due to PbO volatilization during the initial stages of sintering until the PbO vapor pressure above the PZT compact equilibrates with the partial pressure of PbO in the atmosphere. This small loss of Pb suggests that the burial powders are effective in controlling the vapor pressure above the PZT compact, and the amount of Pb lost from the PZT compact during sintering. Furthermore, the high sintering temperatures increase the reactivity of the constituents so that all of the ZrO_2 should go into PZT solid solution. This may not occur, if the calcined powder is initially Pb deficient or if there is significant Pb loss during sintering.

Quantitative image analysis was used to determine the area fraction of monoclinic ZrO_2 in sintered specimens as a function of Pb content. For each specimen, five randomly selected areas were imaged using a BSE microscope. Because of atomic number contrast, ZrO_2 appears darker than bulk PNZT 95/5. However, due to specimen topography from grain pullout, an artifact of specimen preparation, and regions of porosity, the BSE images contained shades of gray similar to ZrO_2 regions (Fig 2a). The grayscale overlap complicated image analyses, because the image analysis software was

often unable to distinguish ZrO_2 from porosity and grain pullout. As a result, a rather labor intensive removal of porosity and grain pullout using image processing software was required. After the removal of porosity and grain pullout, a binary thresholding operation on the grayscale image was performed for area fraction determination of the darker ZrO_2 regions (Fig. 2b). A portion of the porosity (Fig. 2a) is likely from ZrO_2 pullout during polishing; as a result, the absolute fraction of ZrO_2 in PZT cannot be determined with certainty from the micrographs. However, trends relating Pb content to ZrO_2 area fraction have been established based on the residual ZrO_2 in the PZT micrographs.

As with the ZrO_2 wt% in calcined powders, the ZrO_2 area fraction decreased with increasing Pb content (Fig. 3). The 2.74 and 2.15% Pb deficient specimens contained the highest area fraction of ZrO_2 at 0.02. This monoclinic ZrO_2 phase formed during calcination. Perhaps the combination of local Pb deficiency and the refractoriness of ZrO_2 resulted in incomplete incorporation of ZrO_2 into PNZT solid solution during

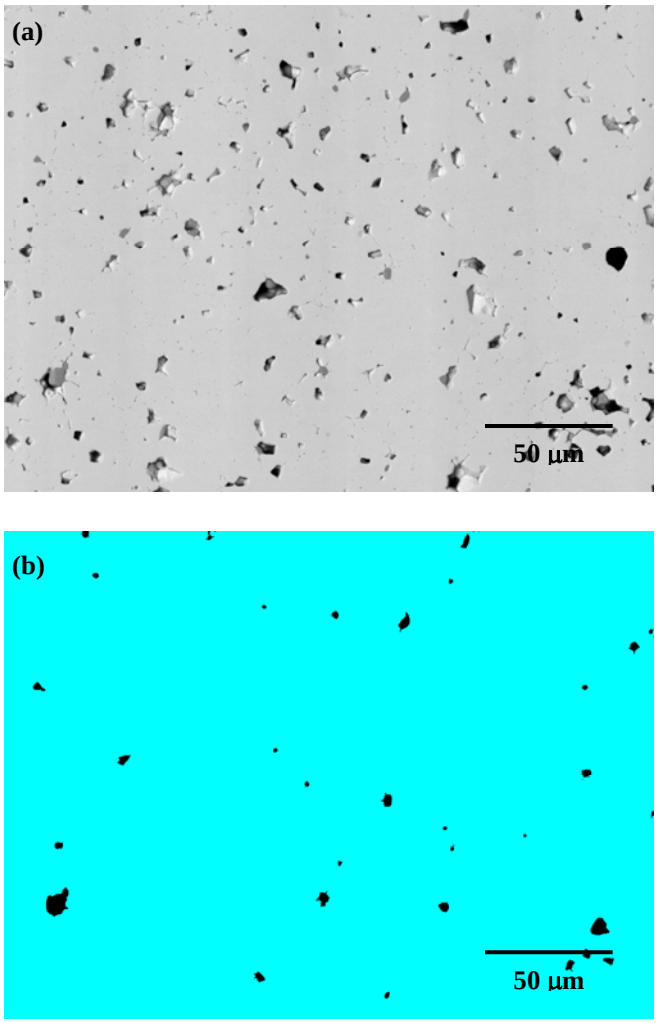

Fig. 2 Example of an (a) original backscattered electron image and (b) the binary image used for image analyses to obtain area fraction of ZrO_2 in polished PNZT 95/5 ceramics.

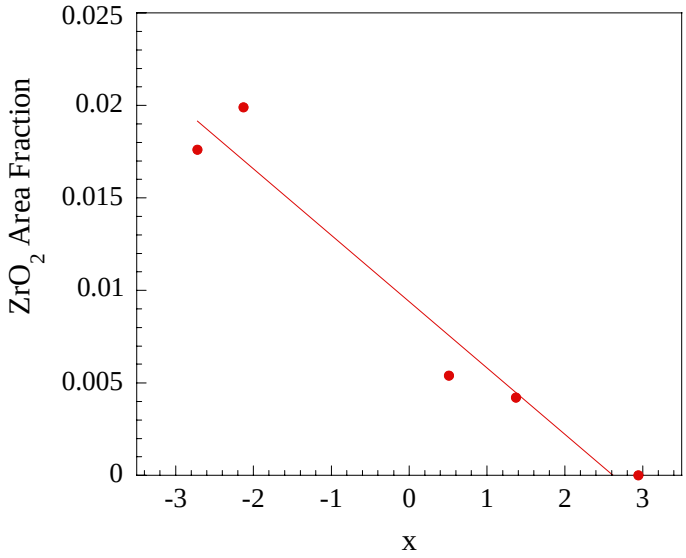

Fig. 3 Area fraction of the monoclinic ZrO_2 second phase decreases with increasing Pb content. The ZrO_2 area fraction data are based on image analyses of cross-sectioned and polished specimens of PNZT 95/5 ceramics.

sintering. At 2.97% excess Pb, no ZrO_2 was found even though monoclinic ZrO_2 was detected in the calcined power using XRD. Yang *et al*[16] suggested that increasing Pb resulted in the incorporation of additional Zr^{4+} into PNZT solid solution. Their hypothesis was supported by structural refinement calculations on calcined powders, which showed an increase in unit cell volume with increasing Pb content, suggesting that additional Zr^{4+} is incorporated in the lattice structure. Decreases in the coercive field and pressure-induced FE-to-AFE phase transformation and increased charge storage capacity provided supporting evidence to their hypothesis. Perhaps, the excess Pb for the 2.97% specimen resulted in the formation of more PbO-rich liquid-phase during sintering thereby enhancing the reaction of any remaining ZrO_2 to form PNZT solid solution.

Fracture Mode

Fracture surfaces were examined with SEM to determine fracture mode (Fig 4). The Pb deficient specimens and the 0.51% and 1.38% Pb excess specimens failed predominantly in a transgranular failure mode (Fig 4a-d); however, the 2.97% Pb excess specimen failed predominantly in an intergranular fracture mode (Fig 4e). Intergranular fracture for the high Pb specimen may be the result of a PbO-rich second phase at grain boundaries leading to weaker grain boundaries. PZT with excess Pb is known to sinter in the presence of a PbO-rich liquid. If the PbO-rich liquid is not depleted due to reaction with other constituents or due to volatilization, upon cooling a PbO-rich second phase will be found at grain boundaries and triple points.[10-12] This second phase can have deleterious effects on the electrical[6] and mechanical properties of PZT. However, excess Pb is needed to help compensate for Pb loss during processing and to enhance the reaction of the ZrO_2 second phase to PZT solid solution. Thus, tight processing control must be maintained in order to achieve stoichiometric levels of Pb in the sintered ceramic.

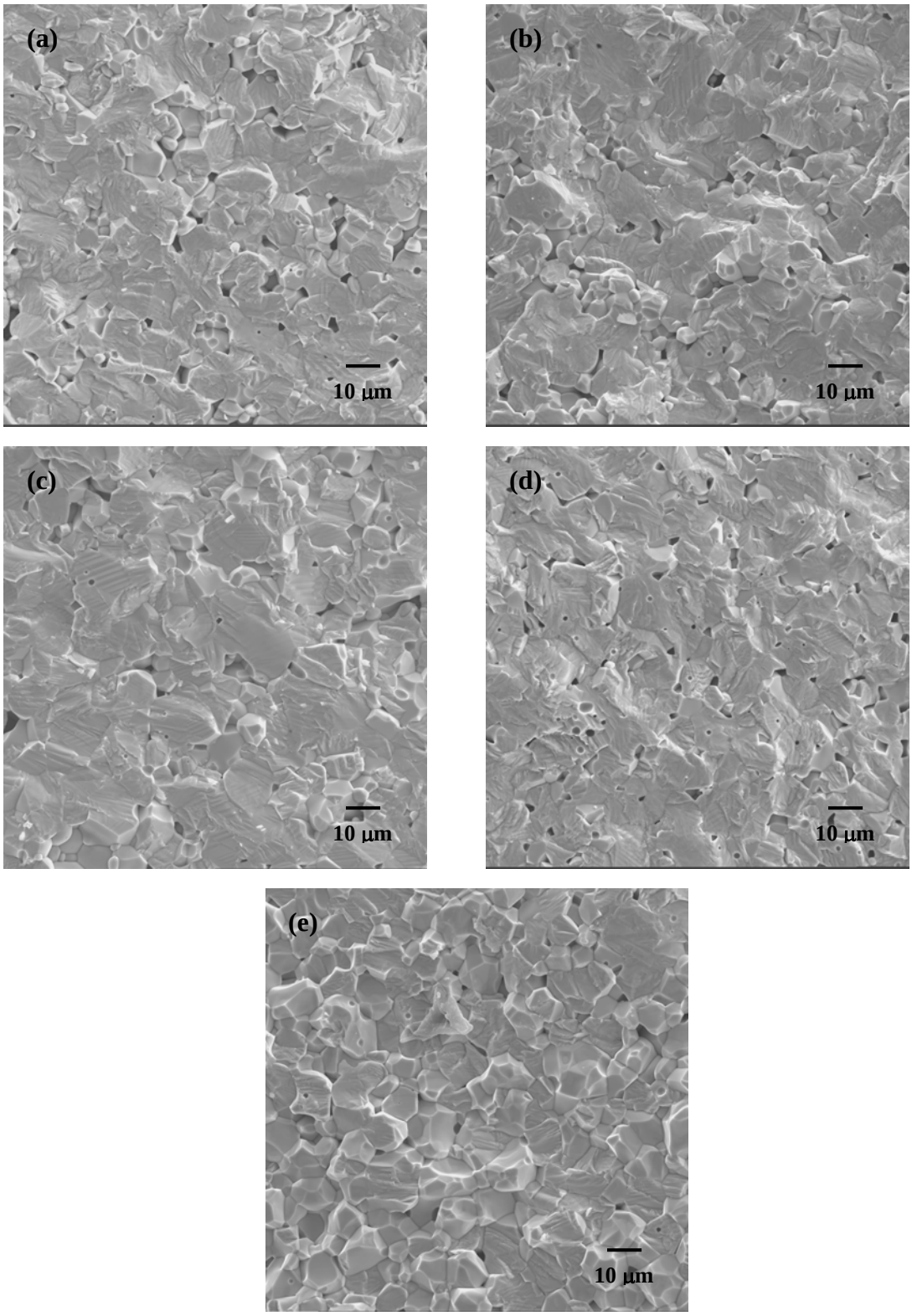

Fig. 4 SEM micrographs showing fracture surfaces of the specimens (a) -2.74, (b) -2.15, (c) 0.51, (d) 1.38 and (e) 2.97% Pb from stoichiometry. The fracture mode is predominately transgranular for all of the specimens except for the 2.97% Pb excess specimen that failed predominately intergranularly.

Grain Size

Grain size measurements were made to determine the effect of Pb content on average grain size and grain size distribution. Optical micrographs of polished and etched PNZT 95/5 ceramics with corresponding binary images for grain size image analyses are shown in Fig. 5. Black areas, which are typically regions of porosity and/or grain pullout, were not included in the grain size measurement routine. The average grain size increased with increasing Pb content (Fig. 6). Similar observations have been made for PZT with increasing Pb content.[7] Two potential sources for the increase in grain size with increasing Pb content include: (i) inhibited grain growth in the presence of a second phase[22] (in this cases there is less ZrO_2 to inhibit grain growth with increasing Pb) or (ii) excess Pb enhanced sintering mechanisms due to increased diffusion of ions in the liquid phase to grains. Although there is a change in grain size, the differences are too small to have a significant impact on the electrical and mechanical properties of PNZT 95/5. Second phases will most likely have the most effect on mechanical properties. Grain size distributions are shown in the Appendix.

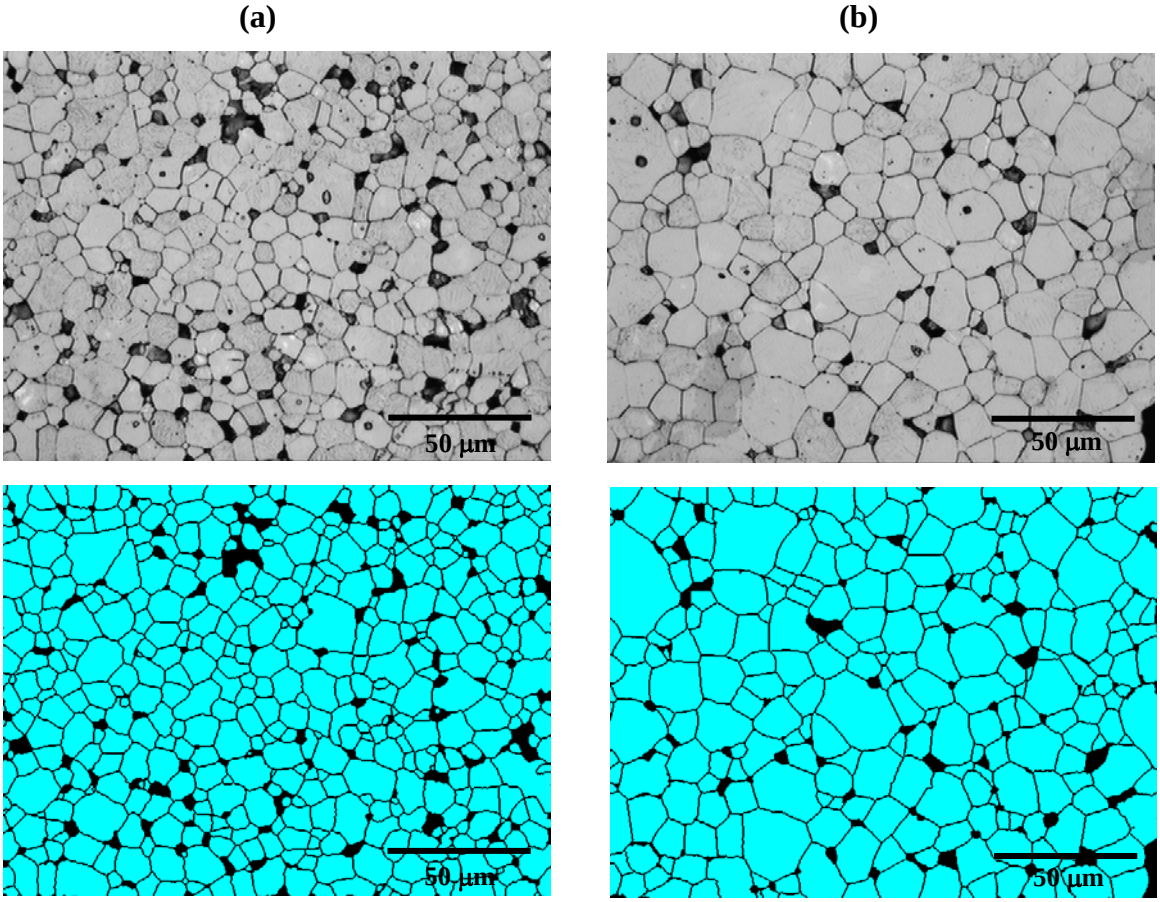

Fig. 5 Optical micrographs of etched PNZT 95/5 ceramics with corresponding binary images for grain size image analyses. A difference in grain size is seen when comparing the (a) low Pb (-2.74%) and the (b) high Pb (2.97%) specimens.

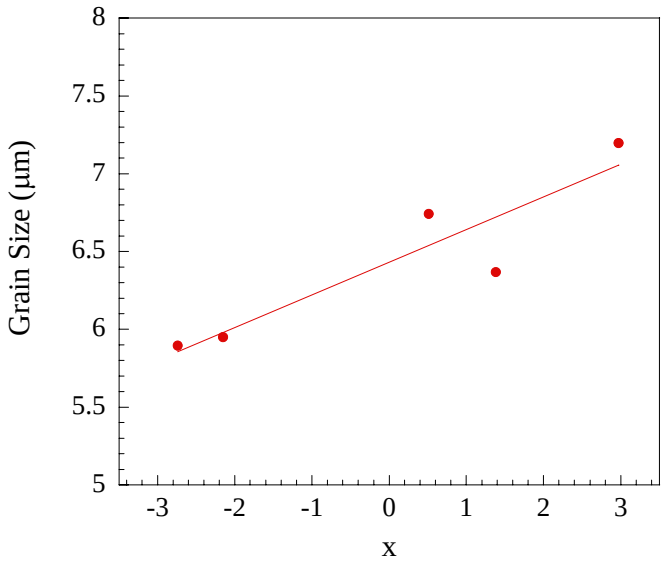

Fig. 6 The average grain size of PNZT 95/5 ceramics increases with increasing Pb content.

Hardness

A total of 10 Vickers indentations was used to determine the hardness of each specimen. Twenty-five to thirty indentations were made per specimen, but many were rejected due to severe multiple cracking, spalling and crushing around the indentations. The hardness did not vary systematically with Pb content (Fig. 7) as did microstructural features (ZrO_2 area fraction, fracture mode and grain size). The hardness ranged between 2.9 and 3.1 GPa. Interestingly, the 0.51% Pb specimen, which is the specimen nearest to stoichiometry, had the highest hardness. The other specimens essentially had the same measured hardness.

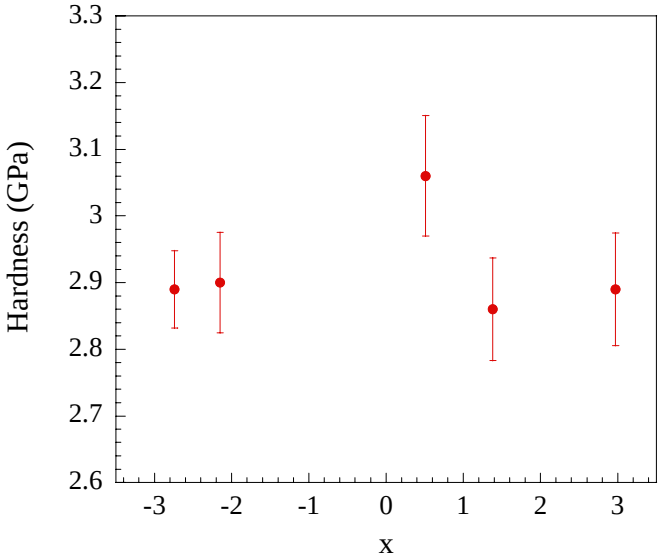

Fig. 7 Vickers hardness with 95% confidence limits does not deviate with increasing Pb content except for the specimen nearest stoichiometry (0.51% excess Pb)

Fracture Toughness

Fracture toughness was determined using the indentation crack-length technique[20] where the toughness measurements were made from the same indentations used for hardness measurements (Fig. 8). Although indentations with the least damage (spalling, crushing and multiple cracking) were used for toughness measurements, most contained some degree of multiple cracking. For indentation crack-length measurements, only one straight crack emanating from the corners of the indentation impression is assumed. Multiple cracking, however, could not be completely eliminated, so only indents with minor multiple cracking were measured. In addition, the indentation crack-length technique is susceptible to systematic errors due to the assumed average geometric and residual stress factors incorporated in Eq 1. As a result, the toughness values should not be used as absolute values, but rather as a gauge for observing toughness trends as a function of processing conditions. The fracture toughness decreased with increasing Pb content from approximately 1.7 to 1.5 $MPa \cdot m^{1/2}$.

Two factors may contribute to the small Pb dependency on fracture toughness: (i) ZrO_2 and (ii) PbO second phases. For instance, the higher ZrO_2 area fraction for the Pb deficient specimens could result in toughening due to crack arrest or due to the presence of the higher toughness second phase. The lower toughness for high Pb containing specimens could be the result of their lower ZrO_2 area fractions. In addition, PZT with excess Pb may have more PbO-rich second phase present at grain boundaries and triple points, leading to lower toughness because of weaker grain boundaries. The decrease in toughness is small within the range of Pb contents (approximately -3 to 3% Pb) examined in this study.

Strength and Weibull Parameters

Flexural strength was measured in four-point bending at room temperature. It is expected that PNZT 95/5 undergoes non-linear stress-strain behavior during loading because of

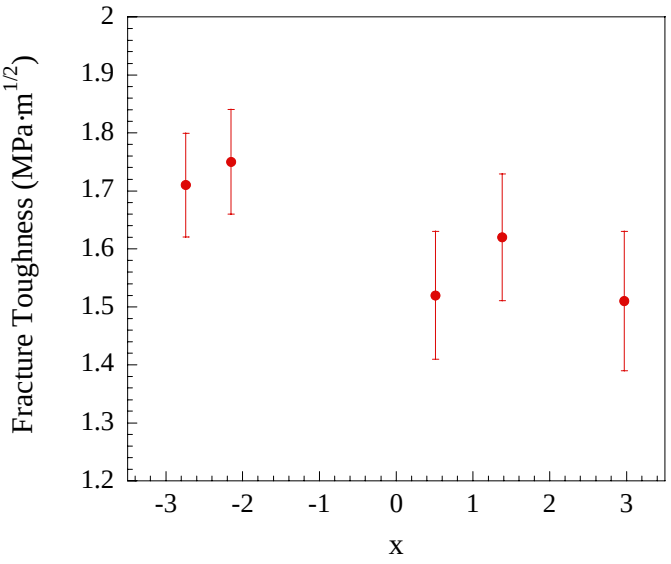

Fig. 8 Plot of fracture toughness as a function of Pb concentration.

domain reorientation during loading.[23] However, load-deflection curves generated from an extensometer indicated that, unlike similar ferroelectric materials, PNZT 95/5 exhibits linear elastic behavior at room temperature. For instance, tin-modified lead zirconate titanate (PSZT) 95/5 exhibited non-linear stress-strain behavior at room temperature, which was enhanced for poled compared to unpoled specimens.[24] The magnitude of non-linearity also increased with temperature. Thus, non-linearity in PNZT 95/5 ceramics may occur for poled specimens and at elevated temperatures. The lack of noticeable non-linearity could also be the result of the small specimen size compounded with the lower resolution associated with extensometers compared to strain gauges. Because non-linearity was not established, failure stress was calculated assuming linear elastic behavior.

The Weibull parameters of PNZT 95/5 were determined to evaluate the effect of Pb stoichiometry on failure stress variability. The failure strength of ceramic materials is dependent on the flaw population and size, which are processing and handling history dependent. Changes in the flaw populations (size, orientation, location, type, distribution) could change the Weibull modulus (m). The Weibull modulus is a statistical parameter used to estimate the variability in strength, which is directly proportional to the failure-initiating flaw distribution within the material. A low Weibull modulus is indicative of a material that exhibits a wide range of failure strengths, and thus has a higher probability of failure at a lower stress level than a material with a similar strength that exhibits a higher Weibull modulus. The Weibull parameters of PNZT 95/5 are needed to determine if changes in microstructure due to differing Pb levels affect failure-initiating flaw distributions and ultimately the failure strength and distributions.

The strength variability was characterized using a two-parameter Weibull distribution and maximum likelihood estimators for Weibull modulus and characteristic strength (σ_0)

$$P_f = 1 - \exp\left[-\left(\frac{\sigma}{\sigma_0}\right)^m\right] \tag{2}$$

where P_f is the probability of fracture. Weibull parameters and the average failure stress are tabulated in Table II. Weibull plots for PNZT 95/5 bend bars containing different Pb concentrations are shown in Fig. 9. No change in the Weibull modulus (m) is observed. This suggests that the flaw distribution does not deviate with changes in the Pb content. As a result, microstructure changes as a function of Pb concentration do not appear to influence the source of failure initiating flaws. Some of the Weibull plots appear to be bimodal distributions, which is indicative of more than one active flaw-type. A systematic examination of failure surfaces has not been attempted, thus the data was not analyzed as more than one flaw population with censored data. Although the failure stress distributions are independent of Pb concentration, there is a slight reduction in strength for the 2.97% Pb specimen (Fig. 10). The strength reduction may be the result of a PbO-rich second phase at the grain boundaries and the slightly lower toughness at the higher lead content.

TABLE II: Weibull Strength Parameters and Average Failure Stress with 95% Confidence Intervals

Percent Pb Excess/Deficient (x)	Weibull Modulus	Characteristic Strength (MPa)	Average Failure Stress (MPa)	Number of Specimens
-2.74	7.7	78.9	73.7 ± 3.2	37
-2.15	7.4	78.9	74.2 ± 3.5	38
0.51	8.2	79.3	74.9 ± 4.0	30
1.38	8.2	73.6	69.4 ± 3.2	38
2.97	8.3	67.5	63.9 ± 3.4	24

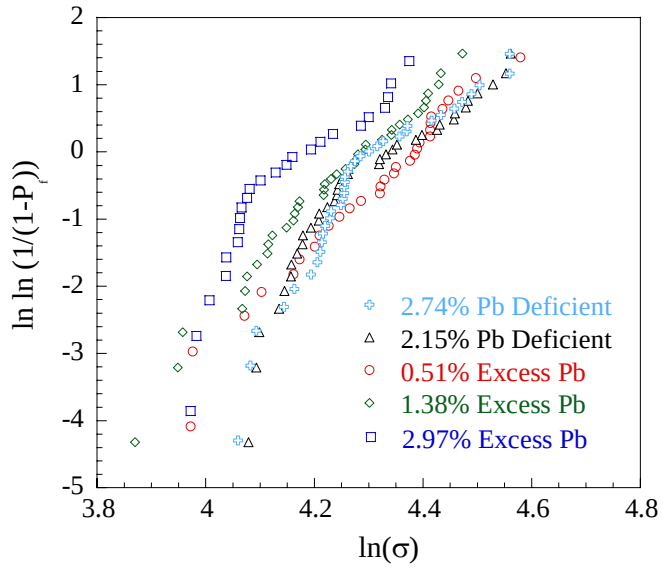

Fig. 9 Weibull plots of failure strength data for PNZT 95/5 ceramics with different Pb contents.

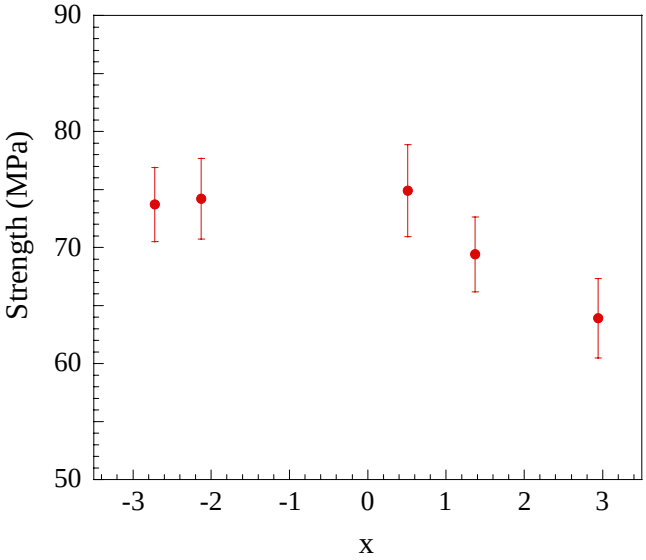

Fig. 10 Average failure stress with 95% confidence intervals for PNZT 95/5 ceramics.

CONCLUSIONS

Pb stoichiometry had appreciable effects on the microstructure and only a modest effect on the mechanical properties of PNZT 95/5 ceramics. Within the limited range of Pb contents examined (approximately -3 to 3% Pb), increased Pb content increases grain size, decreases the formation of monoclinic ZrO_2 second phase and changes the fracture mode from predominately transgranular to intergranular fracture. Although hardness and the Weibull modulus are relatively constant as a function Pb content, strength and fracture toughness both decrease slightly at higher Pb contents. Changes in fracture mode and the slight decrease in the fracture toughness and strength for the 2.97% excess Pb specimens indicate further degradation in the mechanical properties could occur for ceramics with higher concentrations of Pb. Thus, if excess Pb is used to enhance sintering kinetics, to compensate for Pb loss and/or to ensure complete reaction of ZrO_2 into PNZT 95/5 solid solution, then care should be taken to ensure that all of the excess Pb is depleted, either by incorporation into PZT solid solution or by loss due to volatilization.

REFERENCES

1. D. A. Northrop, "Vaporization of Lead Zirconate-Lead Titanate Materials," *J. Am. Ceram. Soc.* **50** [9], 441-445 (1967).
2. R. B. Atkin and R. M. Fulrath, "Point Defects and Sintering of Lead Zirconate-Titanate," *J. Am. Ceram. Soc.* **54** [5], 265-270 (1971).
3. R. L. Holman and R. M. Fulrath, "Intrinsic Nonstoichiometry in Single-Phase $Pb(Zr_{0.5}Ti_{0.5})O_3$," *J. Am. Ceram. Soc.* **55** [4], 192-195 (1972).
4. R. L. Holman and R. M. Fulrath, "Intrinsic Nonstoichiometry in Lead Zirconate Lead Titanate System determined by Knudsen Effusion," *J. Appl. Phys.* **44** [12], 5227-5236 (1973).
5. A. I. Kingon and J. B. Clark, "Sintering of PZT Ceramics: I, Atmosphere Control," *J. Am. Ceram. Soc.* **66** [4], 253-256 (1983).
6. B. M. Song, D. Y. Kim, S. Shirasaki, and H. Yamamura, "Effect of Excess PbO on the Densification of PLZT Ceramics," *J. Am. Ceram. Soc.* **72** [5], 833-836 (1989).
7. S. S. Chiang, M. Nishioka, R. M. Fulrath, and J. A. Pask, "Effect of Processing on Microstructure and Properties of PZT Ceramics," *Am. Ceram. Soc. Bull.* **60** [4], 484-489 (1981).
8. A. I. Kingon, P. J. Terblanche, and J. B. Clark, "The Control of Composition, Microstructure and Properties of $Pb(Zr, Ti)O_3$ Ceramics," *Mater. Sci. Eng.* **71** [1-2], 391-397 (1985).
9. A. I. Kingon and J. B. Clark, "Sintering of PZT Ceramics: II, Effect of PbO Content on Densification Kinetics," *J. Am. Ceram. Soc.* **66** [4], 256-260 (1983).
10. M. A. Akbas, M. A. McCoy, and W. E. Lee, "Microstructural Evolution during Pressureless Sintering of Lead Lanthanum Zirconate-Titanate Ceramics with Excess Lead(II) Oxide," *J. Am. Ceram. Soc.* **78** [9], 2417-2424 (1995).

11. M. Hammer and M. J. Hoffmann, "Sintering Model for Mixed-Oxide-Derived Lead Zirconate Titanate Ceramics," *J. Am. Ceram. Soc.* **81** [12], 3277-3284 (1998).
12. E. K. W. Goo, R. K. Mishra, and G. Thomas, "Transmission Electron-Microscopy of $Pb(Zr_{0.52}Ti_{0.48})O_3$," *J. Am. Ceram. Soc.* **64** [9], 517-519 (1981).
13. A. H. Webster, T. B. Weston, and N. F. H. Bright, "Effect of PbO Deficiency on Piezoelectric Properties of Lead Zirconate-Titanate Ceramics," *J. Am. Ceram. Soc.* **50** [9], 490-491 (1967).
14. R. H. Dungan and L. J. Storz, "Relation between Chemical, Mechanical, and Electrical Properties of Nb_2O_5-Modified 95 Mol% $PbZrO_3$-5 Mol% $PbTiO_3$," *J. Am. Ceram. Soc.* **68** [10], 530-533 (1985).
15. A. Garg and D. C. Agrawal, "Effect of Net PbO Content on Mechanical and Electromechanical Properties of Lead Zirconate Titanate Ceramics," *Mater. Sci. Eng. B-Solid State Mater. Adv. Technol.* **60** [1], 46-50 (1999).
16. P. Yang, J. A. Voigt, S. J. Lockwood, M. A. Rodriguez, G. R. Burns, and C. S. Watson, "The Effects of Lead Stoichiometry on the Dielectric Performance of Niobium Modified PZT 95/5 Ceramics," *Proceedings of the American Ceramic Society Symposium 19: Advanced Dielectric Materials and Multilayer Electronic Devices* **15** (2003).
17. J. A. Voigt, D. L. Sipola, B. A. Tuttle, and M. Anderson, "Nonaqueous Solution Synthesis Process for Preparing Oxide Powders of Lead Zirconate Titanate and Related Materials," *U.S. Patent Number 5 908 802*, June 1, 1999.
18. S. J. Lockwood, E. D. Rodman, S. M. DeNinno, J. A. Voigt, and D. L. Moore, "Chem-Prep PZT 95/5 for Neutron Generator Applications: Production Scale-up Early History," *Sandia National Laboratories Report*, SAND2003-0943 (2003).
19. R. H. Moore, T. V. Montoya, and T. L. Spindle, "Chem-Prep PZT 95/5 for Neutron Generator Applications: Development of Laboratory-Scale Powder Processing Operations," *Sandia National Laboratories Report*, SAND2003-4645 (2003).
20. G. R. Anstis, P. Chantikul, B. R. Lawn, and D. B. Marshall, "A Critical-Evaluation of Indentation Techniques for Measuring Fracture-Toughness: I, Direct Crack Measurements," *J. Am. Ceram. Soc.* **64** [9], 533-538 (1981).
21. P. Yang, B. A. Tuttle, R. H. Moore, J. A. Voigt, T. W. Scofield, and S. J. Lockwood, "Chem-Prep PZT 95/5 for Neutron Generator Applications: The Effect of Pore Former Type and Density on the Depoling Behavior of Chemically Prepared PZT 95/5 Ceramics," *Sandia National Laboratories Report*, SAND2003-3866 (2003).
22. F. F. Lange and M. M. Hirlinger, "Hindrance of Grain-Growth in Al_2O_3 by ZrO_2 Inclusions," *J. Am. Ceram. Soc.* **67** [3], 164-168 (1984).
23. T. Fett, S. Muller, D. Munz, and G. Thun, "Nonsymmetry in the Deformation Behaviour of PZT," *J. Mater. Sci. Lett.* **17** [4], 261-265 (1998).
24. C. S. Watson, "Mechanical Behavior, Properties and Reliability of Tin-Modified Lead Zirconate Titanate," *Sandia National Laboratories Report*, SAND2003-2422 (2003).

APPENDIX

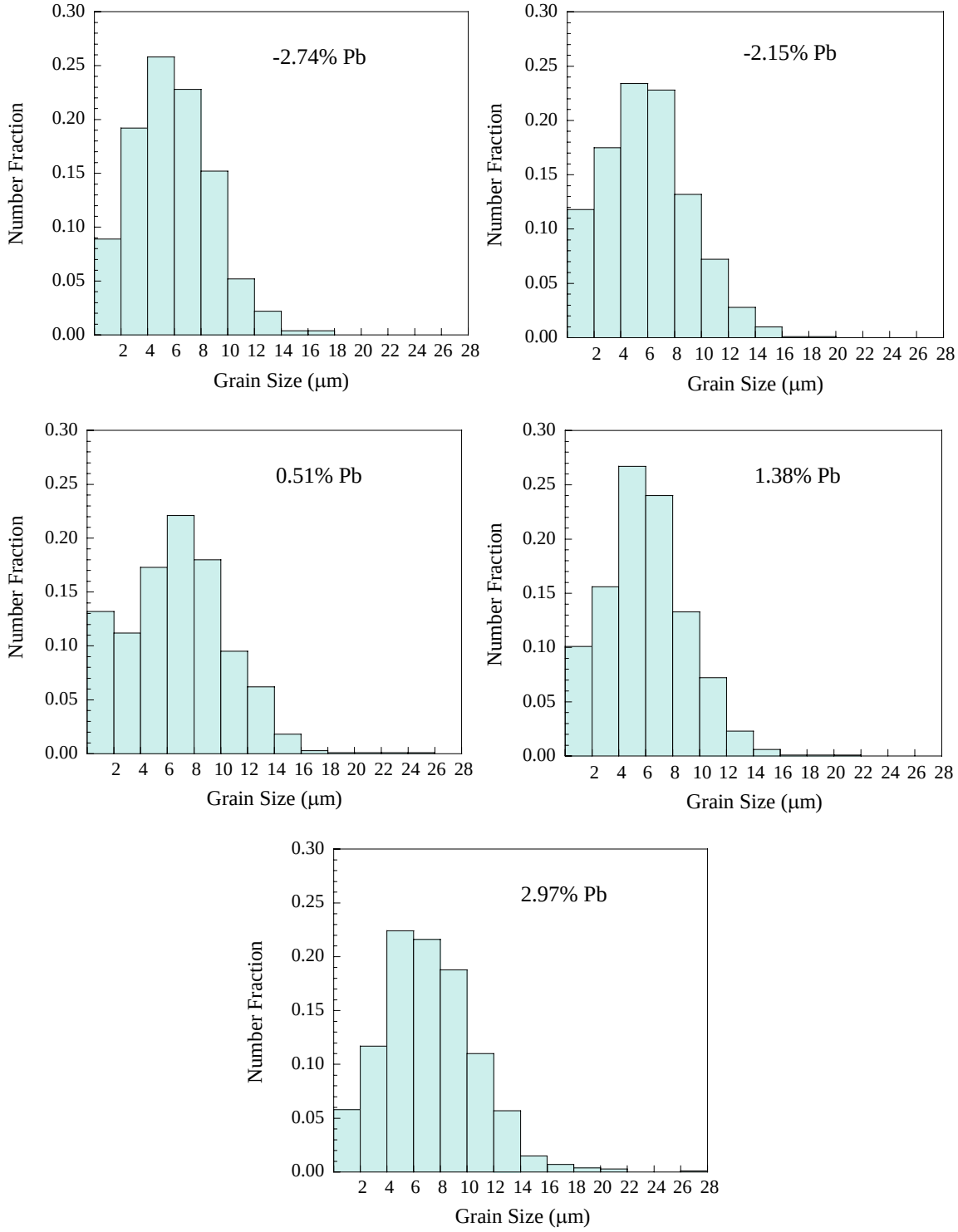

Fig. A Grain size distributions of PNZT 95/5 ceramics with different Pb concentrations. Grain size distributions are similar except the Pb excess specimens exhibit a slight tail for larger sized grains. The number fraction relates the number of grains within a specific size interval and is normalized by the total number of grains counted for the entire analysis.

DISTRIBUTION:

1	MS0378	J. Robbins, 09231
1	0415	D.H. Zeuch, 09741
1	0515	J.D. Keck, 02561
1	0521	S.T. Montgomery, 02561
1	0521	T.W. Scofield, 02561
1	0886	R.P. Grant, 01822
1	0886	A.C. Kilgo, 01822
1	0886	D.F. Susan, 01861
1	0889	S.J. Glass, 01851
1	0889	S.L. Monroe, 01861
1	0889	C. Newton, 01851
1	0889	C.J. Roth, 01851
1	0889	R. Tandon, 01851
1	0959	G.R. Burns, 14154
1	0959	C.B. Diantonio, 14154
1	0959	T.J. Gardner, 14154
1	0959	M.A. Hutchinson, 14154
1	0959	S.J. Lockwood, 14154
1	0959	R.H. Moore, 14154
1	0959	T.V. Montoya, 14154
1	0959	T.L. Spindle, Jr., 14154
1	0959	R.G. Stone, 14154
5	0959	C.S. Watson, 14154
1	0959	P. Yang, 14154
1	0961	C. Adkins, 14150
1	1349	W.F. Hammetter, 01843
1	1349	K.G. Ewsuk, 01843
1	1411	M.V. Braginsky, 01834
1	1411	V. Tikare, 01834
1	1411	B.A. Tuttle, 01851
1	1411	D.L. Moore, 01846
1	1411	M.A. Rodriguez, 01822
1	1411	J.A. Voigt, 01846
1	1411	G.L. Zender, 01822
1	MS9018	Central Technical Files, 8945-1
2	0899	Technical Library, 9616